

A spatially explicit surface urban heat island database for the United States: Characterization, uncertainties, and possible applications

T. Chakraborty^{a,c,*}, A. Hsu^{b,c,d,*}, D. Manya^c, G. Sheriff^e

^a Yale School of the Environment, New Haven, CT, United States

^b Yale-NUS College, Singapore

^c Data-Driven EnviroLab, Singapore

^d School of Public Policy, University of North Carolina-Chapel Hill, NC, United States

^e School of Politics and Global Studies, Arizona State University, Tempe, AZ, United States



ARTICLE INFO

Keywords:

Surface Urban Heat Island Intensity

SUHI

LST

Google earth engine

MODIS

NDVI

Environmental disparities

ABSTRACT

The urban heat island (UHI) effect is strongly modulated by urban-scale changes to the aerodynamic, thermal, and radiative properties of the Earth's land surfaces. Interest in this phenomenon, both from the climatological and public health perspectives, has led to hundreds of UHI studies, mostly conducted on a city-by-city basis. These studies, however, do not provide a complete picture of the UHI for administrative units using a consistent methodology. To address this gap, we characterize clear-sky surface UHI (SUHI) intensities for all urbanized areas in the United States using a modified Simplified Urban-Extent (SUE) approach by combining a fusion of remotely-sensed data products with multiple US census-defined administrative urban delineations. We find the highest daytime SUHI intensities during summer ($1.91 \pm 0.97^\circ\text{C}$) for 418 of the 497 urbanized areas, while the winter daytime SUHI intensity ($0.87 \pm 0.45^\circ\text{C}$) is the lowest in 439 cases. Since urban vegetation has been frequently cited as an effective way to mitigate UHI, we use NDVI, a satellite-derived proxy for live green vegetation, and US census tract delineations to characterize how vegetation density modulates inter-urban, intra-urban, and inter-seasonal variability in SUHI intensity. In addition, we also explore how elevation and distance from the coast confound SUHI estimates. To further quantify the uncertainties in our estimates, we analyze and discuss some limitations of these satellite-derived products across climate zones, particularly issues with using remotely sensed radiometric temperature and vegetation indices as proxies for urban heat and vegetation cover. We demonstrate an application of this spatially explicit dataset, showing that for the majority of the urbanized areas, SUHI intensity is lower in census tracts with higher median income and higher proportion of white people. Our analysis also suggests that poor and non-white urban residents may suffer the possible adverse effects of summer SUHI without reaping the potential benefits (e.g., warmer temperatures) during winter, though establishing this result requires future research using more comprehensive heat stress metrics. This study develops new methodological advancements to characterize SUHI and its intra-urban variability at levels of aggregation consistent with sources of other socioeconomic information, which can be relevant in future inter-disciplinary research and as a possible screening tool for policy-making. The dataset developed in this study is visualized at: <https://datadrivenlab.users.earthengine.app/view/usuhapp>.

1. Introduction

The urban heat island (UHI) effect refers to the phenomenon of higher temperatures in cities and impacts multiple domains, including local weather and climate, energy demand, and public health (Arnfield, 2003; Tan et al., 2010; Santamouris, 2014; Heaviside et al., 2017). UHI intensity can be defined by canopy temperature (CUHI) or surface

temperature (SUHI). CUHI is derived from air temperature (T_a) measurements, while SUHI is based on satellite-derived land surface temperature (LST). Thus, the CUHI and SUHI, while both representing a measure of local temperature perturbations due to urbanization, are not identical, and can have potentially distinct diurnal and seasonal patterns (Arnfield, 2003; Voogt and Oke, 2003; Chakraborty et al., 2017). In general, both background climate and city-specific characteristics,

* Corresponding authors at: Yale School of the Environment, New Haven, CT, United States (T. Chakraborty). Yale-NUS College, Singapore (A. Hsu).

E-mail addresses: tc.chakraborty@yale.edu (T. Chakraborty), angel.hsu@yale-nus.edu.sg (A. Hsu).

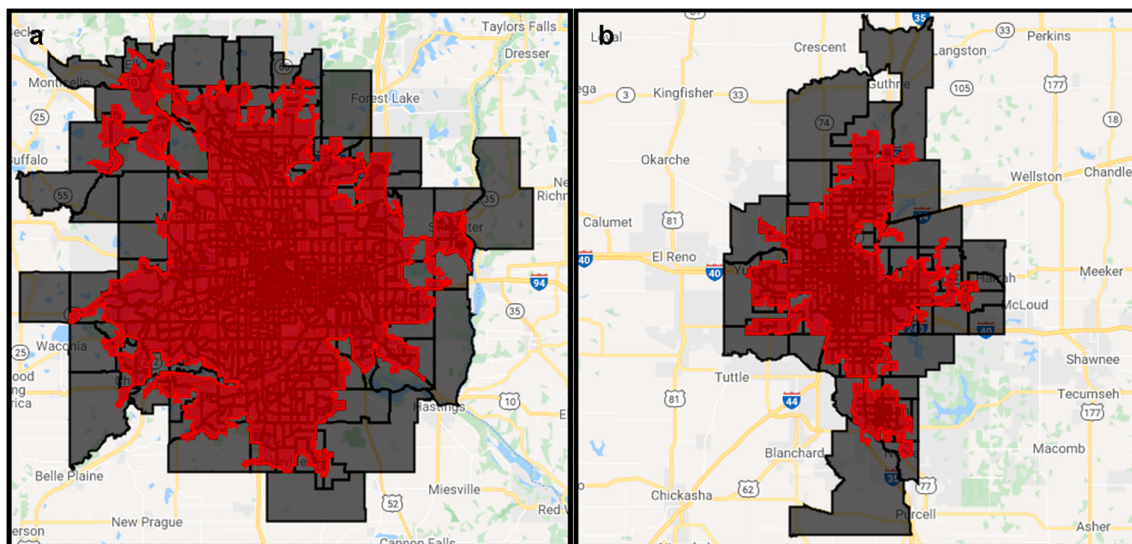


Fig. 1. Examples of the two levels of aggregation used for processing the satellite data for (a) Minneapolis, Minnesota and (b) Oklahoma City, Oklahoma. The red polygons are the urbanized areas used for calculating the average SUHI intensity from the difference in LST between the spectrally classified urban (built-up pixels) and rural (non built-up, non water pixels) references. The black polygons show the groups of census tracts that overlap the urbanized area in each case. Only the satellite data over the urbanized areas (red polygons) are used for SUHI calculations. SUHI value for an inner-city census tract is identical to the average SUHI for the tract, while for the census tracts extending beyond the edge of the urbanized areas, only the pixels in that also overlap the red polygon are considered. The data can be visualized here: <https://datadrivenlab.users.earthengine.app/view/usuhiaapp>.

including the presence (or absence) of urban green space, amount and properties of built-up materials, and intensity of human activity, modulate the UHI's mean intensity and seasonal variability (Peng et al., 2012; Zhao et al., 2014; Chakraborty and Lee, 2019; Manoli et al., 2019). With reference to these factors, the UHI also shows significant intra-city variability since urban areas are highly heterogeneous.

Characterizing the spatial variability in the CUHI requires dense T_a sensor networks in cities. Although the number of such networks is increasing, they are available for few cities and over limited time periods (Muller et al., 2013). In-situ measurements also suffer from considerations of representative placement, variable accuracy, and drift of individual sensors (Stewart 2011). In contrast, satellites have the advantage of monitoring all cities at the global scale using the same sensor, allowing spatially continuous mapping of SUHI. Although this does not imply that satellite-derived SUHI estimates have no uncertainty (Lai et al., 2018), these uncertainties largely stem from the selection of pixels to delineate urban and rural areas (Zhang et al., 2019), as well as the large variabilities in what satellites 'see' over heterogeneous urban terrain (Laguarda et al., 2004; Hu et al., 2016). Even though SUHI and CUHI are not equivalent (Hu et al., 2019), using satellite observations allow us to examine one major impact of urbanization on local climate, as well as its intra-urban variations, in a more consistent manner.

There have been several multi-'city' SUHI studies from the national to the global scale (Peng et al., 2012; Clinton and Gong 2013; Li et al., 2017; Chakraborty and Lee 2019). However, the regions of interest used in these studies do not necessarily make their findings directly implementable from the urban planning perspective. The UHI effect stems from actual physical changes to the Earth's land surfaces, while decision making aims to serve residents within administrative units. Chakraborty and Lee (2019) and Clinton and Gong (2013), for instance, both focus on physical urban agglomerations, not administrative boundaries, which, while important for providing climatological baseline values for clear-sky conditions, limit their application for policymakers who are interested in designing heat mitigation strategies for urban residents at the administrative scale. For global studies, comparing SUHI intensities using administratively determined city delineations is problematic since city definitions vary widely across nations. In general, these cross-city comparisons do not deal with intra-urban variability and instead focus on city-level mean values.

To address these gaps in SUHI comparability, particularly its intra-urban variability, here we focus on the United States and US Census-defined administrative boundaries to create a methodologically consistent database of SUHI intensity. Disaggregating mean satellite-derived SUHI values across census tracts both allows analysis of how SUHI is modulated by other physical characteristics at the tract level and facilitates its combination with socioeconomic information relevant for inter-disciplinary research and applications. To demonstrate the first use, we examine how urban vegetation, elevation, and distance from the coast modulate the annual, summertime, and nighttime SUHI intensity for both day and night across climate zones in the US using a statistical approach. To demonstrate the latter, we provide preliminary evidence of large disparities in SUHI intensity for different income and racial groups in the US. A more detailed analysis of these disparities can be found in Hsu et al. (under review). Given that satellite-derived LST does not represent the climatological mean state and is not equivalent to actual heat exposure or total heat loading, we discuss its limitations in the context of this study. Similar uncertainties are also discussed for the proxy for vegetation cover used. Keeping these limitations in mind, the results have possible applications for future research to further understand the SUHI and its intra-urban variability, as an input to estimate more health-focused metrics of environmental stress in urban areas, and as a potential factor for urban-scale policy-making in the US.

2. Material and methods

2.1. Data sources and regions of interest

We use the following remotely sensed data in the present study:

1. The Moderate Resolution Imaging Spectroradiometer (MODIS) 8-day and daily LST products from NASA's Aqua satellite (MYD11A2 v006 and MYD11A1 v006) at 1000 m resolution from 2013 to 2017 (Wan, 2014)
2. MODIS 8-day surface reflectance product from Aqua satellite (MYD09A1 v006) at 500 m resolution from 2013 to 2017 (Vermote et al., 2011)
3. Global Multi-Resolution Terrain Elevation Data (GMTED) at 30 m resolution from 2010 (Danielson and Gesch, 2011)

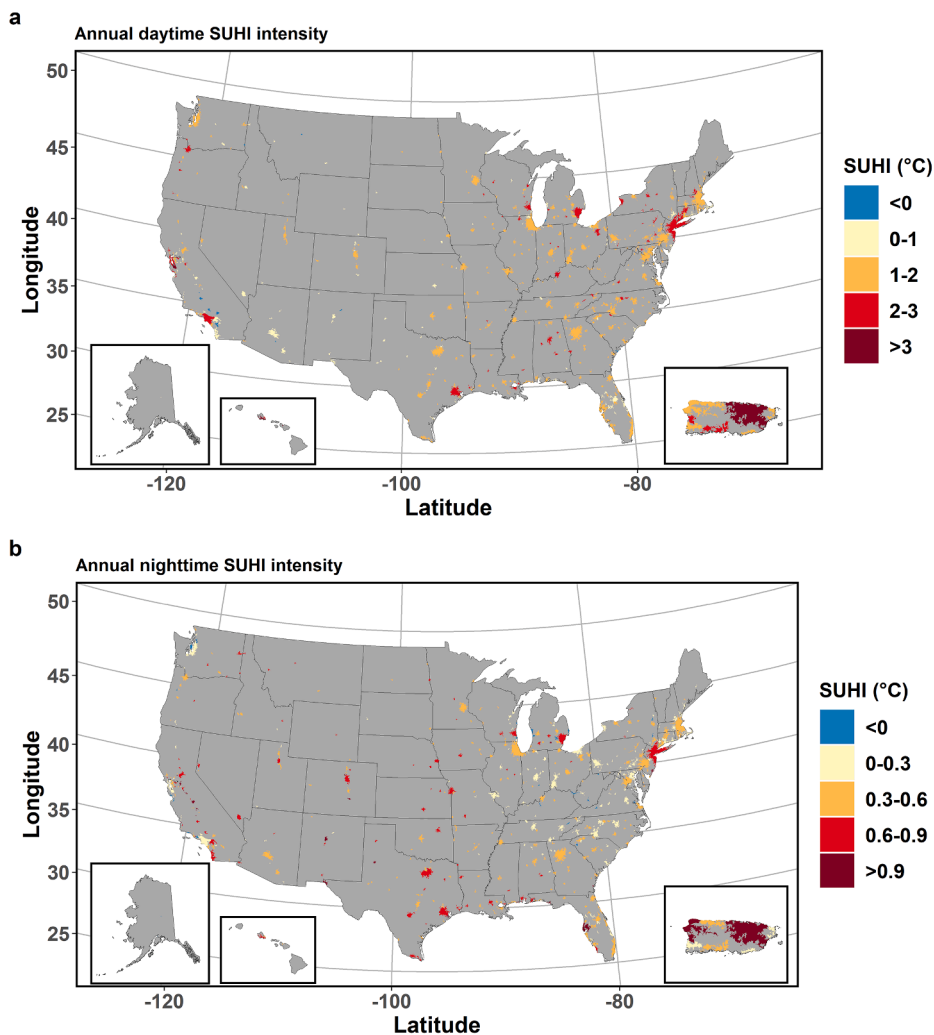


Fig. 2. Map of all urbanized areas in the US, along with their mean (a) annual daytime and (b) annual nighttime SUHI intensity for 2013–2017. The sub-panels include Alaska, Hawaii, and Puerto Rico.

4. European Space Agency's Climate Change Initiative (ESA CCI) land cover data at 300 m resolution for 2015 (Bontemps et al., 2013)
5. National Land Cover Database (NLCD) tree canopy dataset at 30 mm resolution for 2013 (Coulston et al., 2012)

Measurements from the MODIS sensor on the Aqua satellite are chosen over the Terra satellite since the overpass time during the day for Aqua is 1:30 pm local time, which better corresponds to the peak daytime LST. Since the focus is on urban areas, we only consider the census tracts intersecting urbanized areas, which the US census bureau defines as densely settled geographical regions with more than 50,000 residents (<https://www.census.gov/programs-surveys/geography/guidance/geo-areas/urban-rural/2010-urban-rural.html>). Our SUHI data comprise 55,871 census tracts, grouped into 497 urbanized areas (Figs. 1 and 2), covering approximately 78 percent of the U.S. population. Tract-level information on median household income and race (White, Black, Asian, American Indian, Hawaiian, and others) come from the 2017 American Community Survey 5-year Data Profile from 2017 (Mather et al., 2005).

The prevailing background climate for each urbanized area is determined from the Köppen-Geiger dataset (Rubel and Kottek, 2010; Fig. S1), based on the climate zone of the centroid of each of the chosen 497 urbanized areas. Of these, 3 of the centroids do not overlap any of the climate zones due to the coarseness of the Köppen-Geiger dataset, and are designated to have the nearest climate zone. Finally, a census

tract group is considered coastal if the original urbanized area intersects the Natural Earth global coastal dataset at 10 m resolution (<https://www.naturalearthdata.com/downloads/10m-physical-vectors/10m-coastline/>). All spatial analyses are done on the Google Earth Engine platform (Gorelick et al., 2017).

2.2. Satellite data processing

We pre-processed the 8-day LST images to exclude pixels with an uncertainty of more than 3 °C, based on the pixel-level quality control flags, similar to Chakraborty and Lee (2019). The use of 8-day images versus daily LST data prevents sampling biases due to differing overcast periods across regions of the country (see Discussion). Similarly, we use the highest-quality pixels of the MODIS 8-day surface reflectance product to compute the Normalized Difference Vegetation Index (NDVI) (Rouse et al., 1974):

$$\text{NDVI} = (\text{NIR} - \text{RED}) / (\text{NIR} + \text{RED}), \quad (1)$$

where NIR and RED are the surface reflectance in the near infrared (band 2) and red (band 1). We extract terrain elevation from the Dangelson and Gesch (2011) Digital Elevation Model (DEM).

Annual LST and NDVI values are simple means of all 8-day images from 2013 to 2017, while seasonal values are means from June to August (summer) and December to February (winter). Since sensors do not penetrate clouds, annual or seasonal values should be considered

Table 1

Summary of calculated SUHI intensities (mean \pm standard deviation) for the cases considered in the present study. These values are not weighted by area.

SUHI	Case	Regions of interest				
		All US	Arid	Boreal	Temperate	Tropical
Annual daytime (°C)	All	1.38 \pm 0.66	0.5 \pm 0.57	1.55 \pm 0.56	1.39 \pm 0.58	2.03 \pm 0.87
	Coastal	1.46 \pm 0.77	0.23 \pm 0	1.25 \pm 0.54	1.36 \pm 0.68	2.1 \pm 0.9
	Non-Coastal	1.36 \pm 0.63	0.5 \pm 0.58	1.56 \pm 0.56	1.4 \pm 0.55	1.58 \pm 0.64
Annual nighttime (°C)	All	0.4 \pm 0.28	0.64 \pm 0.3	0.35 \pm 0.27	0.39 \pm 0.26	0.56 \pm 0.35
	Coastal	0.42 \pm 0.34	0.64 \pm 0	0.1 \pm 0.19	0.4 \pm 0.33	0.59 \pm 0.36
	Non-Coastal	0.4 \pm 0.27	0.64 \pm 0.3	0.35 \pm 0.27	0.38 \pm 0.24	0.35 \pm 0.04
Summer daytime (°C)	All	1.91 \pm 0.97	0.52 \pm 0.82	2.1 \pm 0.8	2.01 \pm 0.9	2.22 \pm 0.99
	Coastal	1.98 \pm 0.99	-0.27 \pm 0	1.95 \pm 0.61	1.95 \pm 0.97	2.29 \pm 1.01
	Non-Coastal	1.89 \pm 0.97	0.54 \pm 0.82	2.1 \pm 0.81	2.02 \pm 0.88	1.69 \pm 0.84
Summer nighttime (°C)	All	0.6 \pm 0.27	0.74 \pm 0.33	0.61 \pm 0.24	0.57 \pm 0.26	0.62 \pm 0.35
	Coastal	0.53 \pm 0.31	0.58 \pm 0	0.28 \pm 0.22	0.52 \pm 0.3	0.65 \pm 0.37
	Non-Coastal	0.62 \pm 0.25	0.75 \pm 0.33	0.62 \pm 0.23	0.59 \pm 0.24	0.39 \pm 0.05
Winter daytime (°C)	All	0.87 \pm 0.45	0.54 \pm 0.4	0.9 \pm 0.41	0.86 \pm 0.39	1.75 \pm 0.77
	Coastal	0.98 \pm 0.67	0.74 \pm 0	0.6 \pm 0.43	0.84 \pm 0.52	1.8 \pm 0.8
	Non-Coastal	0.85 \pm 0.39	0.54 \pm 0.4	0.91 \pm 0.41	0.87 \pm 0.35	1.39 \pm 0.5
Winter nighttime (°C)	All	0.31 \pm 0.34	0.52 \pm 0.31	0.34 \pm 0.38	0.25 \pm 0.31	0.47 \pm 0.34
	Coastal	0.35 \pm 0.4	0.7 \pm 0	0.01 \pm 0.27	0.33 \pm 0.4	0.5 \pm 0.35
	Non-Coastal	0.3 \pm 0.33	0.51 \pm 0.31	0.35 \pm 0.38	0.22 \pm 0.27	0.25 \pm 0.05

clear-sky estimates. We use the ESA CCI land cover data for 2015 since it is in the middle of the 2013–2017 range. All satellite data are processed at 300 m resolution to be consistent with the land cover data.

2.3. SUHI and Urban-Rural differential estimation at multiple levels of aggregation

We use the Simplified Urban Extent (SUE) algorithm, originally developed to characterize SUHI intensity in a globally consistent manner (Chakraborty and Lee, 2019), to calculate the annual, summer, and winter SUHI intensities for day and night. Traditional SUHI estimates usually assume a fixed buffer around an urban region of interest to create a rural reference and compare the temperature differential between the two (Clinton and Gong, 2013). The footprint of the SUHI, however, can vary widely between cities (Zhou et al., 2015; Yang et al., 2019), preventing a standard method to select a rural reference based on these buffers. This lack of standardization is more problematic when using administrative boundaries since a hypothetical buffered region around these boundaries may or may not be built-up. To address these issues, the SUE method defines the SUHI as the average LST difference between the urban and non-urban pixels, as classified from spectral reflectance data, within an urban agglomeration or city (Chakraborty and Lee, 2019).

The US Census Bureau's 497 urbanized areas are our urban agglomerations, while we use ESA CCI pixel-level data to delineate urban and rural references. Thus, the rural reference includes all non-urban, non-water land cover classes within each urbanized area. Although results from the SUE algorithm have been independently validated against both observational and theoretical estimates of SUHI intensity (Manoli et al., 2020a; Niu et al., 2020), there is debate regarding whether it constitutes a 'true' rural reference (for an extended discussion, see Chakraborty and Lee (2019)). For the purposes of this study, however, SUHI intensity is the average LST difference between the average built-up pixel and the average non built-up pixel within each urbanized area. While a similar method of delineating urban and rural references would not work for CUHI, this is primarily due to the stronger effect of advection on T_a compared to LST. Similar to the algorithm used for SUHI, we also calculate urban–rural differentials in NDVI (Δ NDVI) and DEM (Δ DEM) for each agglomeration. To examine the suitability of using NDVI as a proxy for vegetation, we calculate the urban–rural differential in tree cover percentage (Δ Tree Cover) for each urbanized area from the NLCD dataset (see Discussion).

To calculate SUHI and urban–rural differentials for a census tract, we keep the rural reference identical (based on the non-urban, non-water

ESA CCI pixels within the urbanized area), while all pixels within the urbanized part of the census tracts are used as the urban reference. This is a necessary modification to the SUE algorithm to account for the mismatch between the physical extent of an urban area and its administrative boundaries (Hsu et al., 2018; Chakraborty et al., 2019). Though this adjustment does not keep both remotely sensed and socioeconomic data at the same level of aggregation, we assume that most people live in the part of the census tract contained in the urbanized area. Moreover, using all pixels within the urbanized area of the census tract gives a more complete picture of the average LST of the tract, accounting for presence (or absence) of green space, bare soil, permanent snowpack, etc. Fig. 1 shows two examples of these different levels of aggregation used in this study.

3. Results

3.1. Spatial and seasonal variability in SUHI in the US

Fig. 2 shows a map of US urbanized areas including their mean annual clear-sky daytime and nighttime SUHI intensities. The annual average SUHI intensity is 1.38 ± 0.66 °C during daytime and 0.40 ± 0.28 °C for nighttime. Seasonally, summers show the highest values (1.91 ± 0.97 °C for daytime; 0.60 ± 0.26 °C for nighttime), while winters show the lowest (0.87 ± 0.45 °C for daytime; 0.31 ± 0.34 °C at night; Table 1). The summer SUHI is higher than the annual mean SUHI in $\sim 84\%$ (418/497) of the cases, while the winter SUHI is higher in only $\sim 12\%$ (58/497) cases. This seasonal trend of higher summer SUHI intensities compared to winter values is consistent with previous results - both global and US-specific (Imhoff et al., 2010; Peng et al., 2012; Li et al., 2017; Chakraborty and Lee 2019), and show similar magnitude to the 15-year mean urban cluster-based values extracted from the dataset created by Chakraborty and Lee (2019) (Table S1). Note that the slightly higher SUHI values in the present study are due to primarily two reasons:

1. The global dataset uses a fusion of Terra and Aqua data, with Aqua, which we use in the present study, generally showing higher daytime SUHI values (Chakraborty and Lee, 2019).
2. We focus on urbanized areas, and thus filter out many smaller urban areas with lower expected SUHI values (Zhou et al., 2017).

When divided into climate classes, there is a marked difference in daytime SUHI intensity between arid and other climate zones. Urbanized areas in the arid climate zone show the lowest SUHI intensities

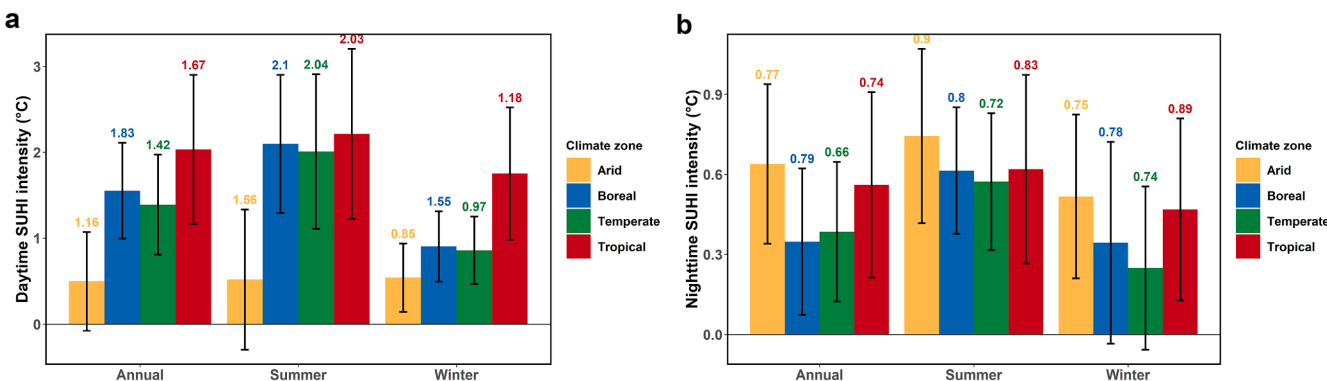


Fig. 3. Bar charts showing 2013–2017 mean annual, summer, and winter daytime (a) and nighttime (b) SUHI intensity of the urbanized areas for each climate zone. The error bars represent the standard deviation of the mean urban daytime SUHI for each case, while the number at the top of the bars represent the pooled standard deviation of intra-urban daytime SUHI intensity for the respective cases.

while those in tropical regions show the highest, both with little seasonal variation. Urbanized areas in temperate and boreal climates show larger seasonal variations. Arid zones also show the lowest intra-urban spatial variation in daytime SUHI intensity for all cases (Fig. 3). During nighttime, urbanized areas in arid climate show the highest SUHI intensity (Fig. 3b).

Although these trends are consistent with global patterns, US-specific characteristics of urbanization affect some results. With a primarily continental climate, the US contains 298 temperate urbanized areas, with only 16 in tropical climate, most of which are on islands, either in Hawaii or Puerto Rico. Values in the temperate zone therefore skew the average SUHI intensities. Moreover, since only one of the 44 arid urbanized areas, San Diego, CA, adjoins the coast, the low SUHI intensity in arid areas leads to a higher overall annual SUHI intensity for coastal urbanized areas (1.46 ± 0.77 °C for coastal; 1.36 ± 0.63 °C for non-coastal), which is counter-intuitive, given the moderating influence of sea breezes on daytime coastal temperature (Santamouris et al., 2017). This expected influence of sea-breeze moderation on SUHI emerges when this analysis is done separately for temperate (1.36 ± 0.68 °C for coastal; 1.40 ± 0.55 °C for non-coastal) and boreal (1.25 ± 0.54 °C for coastal; 1.56 ± 0.60 °C for non-coastal) urbanized areas. This result is mostly consistent for summer and winter SUHI intensities (Table 1). During nighttime, when one would expect coastal areas to have relatively higher temperatures, summer SUHI intensity is actually higher for non-coastal urbanized areas (0.53 ± 0.31 °C for coastal; 0.62 ± 0.25 °C for non-coastal). This difference is not due to a sampling issue since we essentially analyze all urbanized areas, as defined by the US census bureau. While it is possible to extend this analysis to the ‘urban areas’, which the US census bureau defines as regions with a population of less than 50,000 people, some of these tend to be very small, with few census tracts. The limited size and intra-area variation limits the both the ability to obtain sufficient representative pixels to reliably calculate SUHI intensity and to conduct analysis regarding its relationship with socioeconomic variables.

3.2. SUHI intensity and urban green space

Replacement of natural vegetation with impermeable surfaces is a key cause of the urban heat island effect. Although it is one of many factors that controls SUHI (Peng et al., 2012; Zhao et al., 2014), we focus on this land cover conversion due for three main reasons: it has significant intra-urban and inter-urban variation (Cui and De Foy, 2012; Chakraborty and Lee, 2019; Chakraborty et al., 2019); access to green space has been found to be inversely correlated with income (Hsu et al., 2018; Nesbitt et al., 2019; Chakraborty et al., 2019); and urban re-vegetation is a commonly proposed urban heat mitigation strategy (Maimaitiyiming et al., 2014; Ziter et al., 2019). The presence of green

vegetation has other co-benefits beyond reducing local temperature (Dadvand et al., 2015; Fong et al., 2018; Iyer et al., 2020). Finally, given the multiple economic and social benefits of urban forestry (Nowak and Dwyer, 2007), planting urban trees can be easily implementable and defensible from the policy standpoint.

We find daytime SUHI intensity and the urban–rural differential in NDVI (Δ NDVI), a proxy for live green vegetation, to be negatively correlated both within and between urbanized areas (Fig. 4), except for the boreal climate. These correlations are especially strong during summer, which is expected due to higher potential evaporative cooling from vegetated surfaces during this season (Manoli et al., 2020a). Overall, negative correlations persist for 459, 481, and 368 of the 497 urbanized areas for the year, summer, and winter, respectively. Across all urbanized areas, correlations are stronger for non-coastal areas (annually, $r = -0.42 \pm 0.45$ for coastal and -0.66 ± 0.45 for non-coastal urbanized areas after Fisher’s z transformation and back-transformation). This difference may be due to the mediating effect of sea breezes (Santamouris et al., 2017). For temperate climate, which has a large number of both coastal and inland urbanized areas, the difference in correlations is even stronger (annually, $r = -0.41 \pm 0.46$ for coastal and -0.75 ± 0.38 for non-coastal urbanized areas), particularly for summer ($r = -0.50 \pm 0.46$ for coastal and -0.80 ± 0.36 for non-coastal urbanized areas).

Although the overall trends persist during nighttime (Fig. 4d–f), the strengths of the negative correlations are much lower, expected due to the lower differential of (and absolute) evaporative cooling at night (De Dios et al., 2015). In particular, at night, the control of Δ NDVI on inter-urban variation in SUHI practically disappears. A negative trend in SUHI and Δ NDVI is found in 400, 456, and 319 urbanized areas for the year, summer, and winter, respectively and the correlations for non-coastal urbanized areas decrease the most to -0.32 ± 0.37 ($r = -0.40 \pm 0.38$ for coastal urbanized areas).

3.3. SUHI intensity and distance from the coast

We examine the coastal influence on SUHI intensity by calculating the mean and standard deviation of the correlation coefficients (after Fisher’s z transformation and back-transformation) between the distance of the census tract centroids from the nearest coast and the annual, summer, and winter SUHI intensities (Table 2). This analysis is only done for the 110 census tract groups adjoining the coast. On average, the correlation coefficients are negative for both daytime (-0.09 ± 0.42 for annual) and nighttime (-0.5 ± 0.43 for annual). The strong negative correlations are expected during nighttime due to the thermal inertia of water. We examine the correlation coefficients between distance from the coast and Δ NDVI to resolve the seemingly counter-intuitive decreasing daytime SUHI with distance from the coast. For all cases

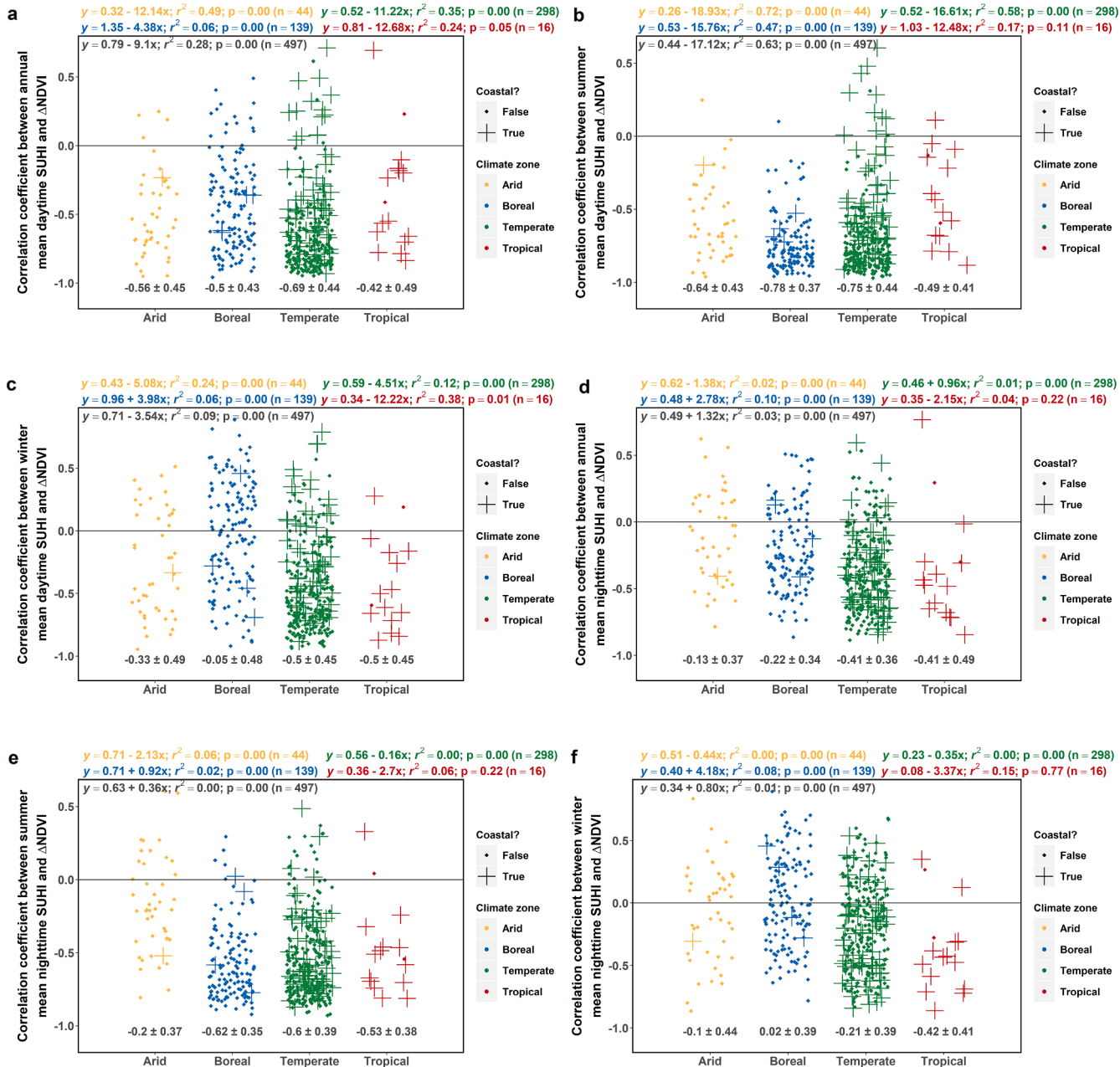


Fig. 4. Summary of intra-urban and inter-urban correlation between 2013 and 2017 (a) daytime SUHI and mean annual ΔNDVI , (b) daytime SUHI and mean summer ΔNDVI , (c) daytime SUHI and mean winter ΔNDVI , (d) nighttime SUHI and mean annual ΔNDVI , (e) nighttime SUHI and mean summer ΔNDVI , and (f) nighttime SUHI and mean winter ΔNDVI . The points show the distribution (jittered) of the Pearson correlation coefficient (r) between the two variables for every US urbanized area divided into the climate zones, calculated from the census tract-level calculations. The numbers below the points give the mean and standard deviation of r after Fisher's z transformation and back-transformation. The equations at the top show the correlations between the variables, calculated from the mean for each urbanized area (in black) and also sub-divided into the climate zones.

Table 2

Correlation (and partial correlation) coefficients between distance of census tract centroid from coast and the variables of interest for all the coastal urban census tract groups. Note that ΔNDVI has no diurnal variation.

Time	Period	SUHI	ΔNDVI	SUHI (accounting for ΔNDVI)
Daytime	Annual	-0.09 ± 0.42	0.28 ± 0.33	0.02 ± 0.4
	Summer	-0.09 ± 0.41	0.28 ± 0.33	0.03 ± 0.4
	Winter	-0.13 ± 0.44	0.29 ± 0.3	-0.07 ± 0.42
Nighttime	Annual	-0.5 ± 0.43	0.28 ± 0.33	-0.45 ± 0.42
	Summer	-0.49 ± 0.46	0.28 ± 0.33	-0.44 ± 0.45
	Winter	-0.48 ± 0.42	0.29 ± 0.3	-0.44 ± 0.41

considered, ΔNDVI is positively correlated with distance from the coast (around 0.28 ± 0.33 for all cases). This means that for the coastal urbanized areas in the US, vegetation density tends to increase farther from the waterfront, thereby counteracting the coastal influence on SUHI. Partial correlations that account for the ΔNDVI variability gives us slightly positive correlation coefficients between SUHI intensity and distance from the coast, at least for the annual and summer cases. It should be noted that isolating the influence of coastal advection on UHI intensity is much more complicated than can be inferred from the bulk statistical analysis performed here and requires considerations of wind speed and direction, land-sea thermal gradients, and other meteorological variables.

3.4. Census-tract elevation: a possible confounding factor

Since temperature varies with altitude, comparing UHI intensities at different elevations is not ideal. The UHI literature typically accounts for this limitation by setting elevation differential thresholds for entire cities (in multi-city analysis) or for individual pixels before calculating SUHI. For illustration, we examine the relationship between SUHI intensity and the urban–rural elevation differential (ΔDEM) for each urbanized area (Fig. S2). The elevation differential is indeed important, showing a negative correlation with SUHI intensity for a slight majority of the urbanized areas considered. Though there is not as much inter-seasonal trend, roughly two-thirds of urbanized areas (316 for year, 320 for summer, and 342 for winter) demonstrate this negative correlation, confirming that census tracts with a higher average elevation have lower temperature. The negative correlations are slightly lower at night. While elevation is an unwelcome confounder when dealing with SUHI intensity itself, it is less problematic from a human welfare perspective. Since it is not necessarily true that higher elevation areas will not be inhabited, using such elevation thresholds in the present study would mask out entire census tracts or large parts of the population who live in the higher elevation regions of the urbanized areas. Therefore, with the aim of consistent assessment of SUHI's local distribution as a bulk parameter, we do not use elevation thresholds, acknowledging that this omission leads to some uncertainties in urbanized areas with large terrain gradients.

3.5. Applications of dataset: exploring SUHI by income and race

Chakraborty et al. (2019) found SUHI to be higher in poorer neighborhoods for the majority of a sample of 25 global cities. Recent studies have explored similar disparities in environmental stressors and access to resources in the US (Clark et al., 2014; Tessum et al., 2019; Hoffman et al., 2020). Here we expand on those studies, demonstrating one use of this dataset by exploring the statistical associations between SUHI intensity, income, and race using a spatially explicit approach. Unlike Chakraborty et al. (2019), which focused on annual mean daytime values, we also consider the seasonal and diurnal components of the disparities in SUHI intensity.

Fig. 5 shows the statistical relationship between SUHI intensity and median income for all urbanized areas. SUHI intensity is negatively associated with median income for 436 (~88%), 445 (~89%), and 428

(~86%) of the 497 urbanized areas during the year, summer, and winter, respectively. For all seasons, the strengths of the correlations are highest for the boreal climate, followed by temperate and arid climate. The correlations for the tropical urbanized areas show a fairly even spread from negative to positive. Nighttime SUHI intensity also shows negative, albeit weaker, correlations with median income (Fig. 5d–f).

Mean daytime SUHI intensity is negatively correlated with the percentage of white population for most urbanized areas (i.e., census tracts with higher proportion of white residents have lower SUHI; Fig. 6 shows the patterns for summer). Overall, white is the only racial group for which the mean correlation between SUHI intensity and proportion of population is negative, while the mean positive correlation is highest for the black racial group. These patterns persist even after accounting for income, as seen from the distribution of partial correlation coefficients between the two variables (Fig. 6b). For winter nights, the association between SUHI intensity and race practically disappears (Fig. 6c), especially after accounting for income (Fig. 6d).

Even though absolute temperature may be a more relevant indicator of environmental stress than urban–rural differentials, such as a UHI metric (Martilli et al., 2020a), here we use SUHI to examine environmental disparities for two main reasons:

1. First, it keeps the analysis consistent with the SUHI characterization, which is important from a meteorological perspective because of its impact on local weather and boundary layer processes.
2. Second, since cities are located in a wide variety of climates, the UHI remains a useful proxy to isolate the impact of urbanization on local temperatures (Manoli et al., 2020a), which can be a relevant target for policy interventions.

Since the SUHI is just the difference between the census-tract LST and a constant rural reference LST within each urbanized area, all intra-urban statistical correlations also hold true for the corresponding LST. Accordingly, the use of SUHI in the manuscript (and UHI in general) refers to the additional impacts of urbanization (Heaviside et al., 2017). A more comprehensive discussion on the relevance of the SUHI as an urban heat metric can be found in Martilli et al. (2020b) and Manoli et al. (2020b). Recognizing the importance of LST distinct from SUHI, in addition to our web application visualizing SUHI data (<https://datadrivenlab.users.earthengine.app/view/usuhiaapp>), we have made available a companion data set containing urban and rural LST, NDVI, and DEM estimates for all urbanized census tracts in the US (Chakraborty et al., 2020).

4. Discussion

4.1. Limitations of satellite-derived estimates of urban heat and vegetation

Satellite-derived estimates offer larger scale coverage than ground-based observations but have several limitations relevant to our analysis:

- i) Estimates are only valid for clear-sky conditions and influenced by the scale of temporal aggregation;

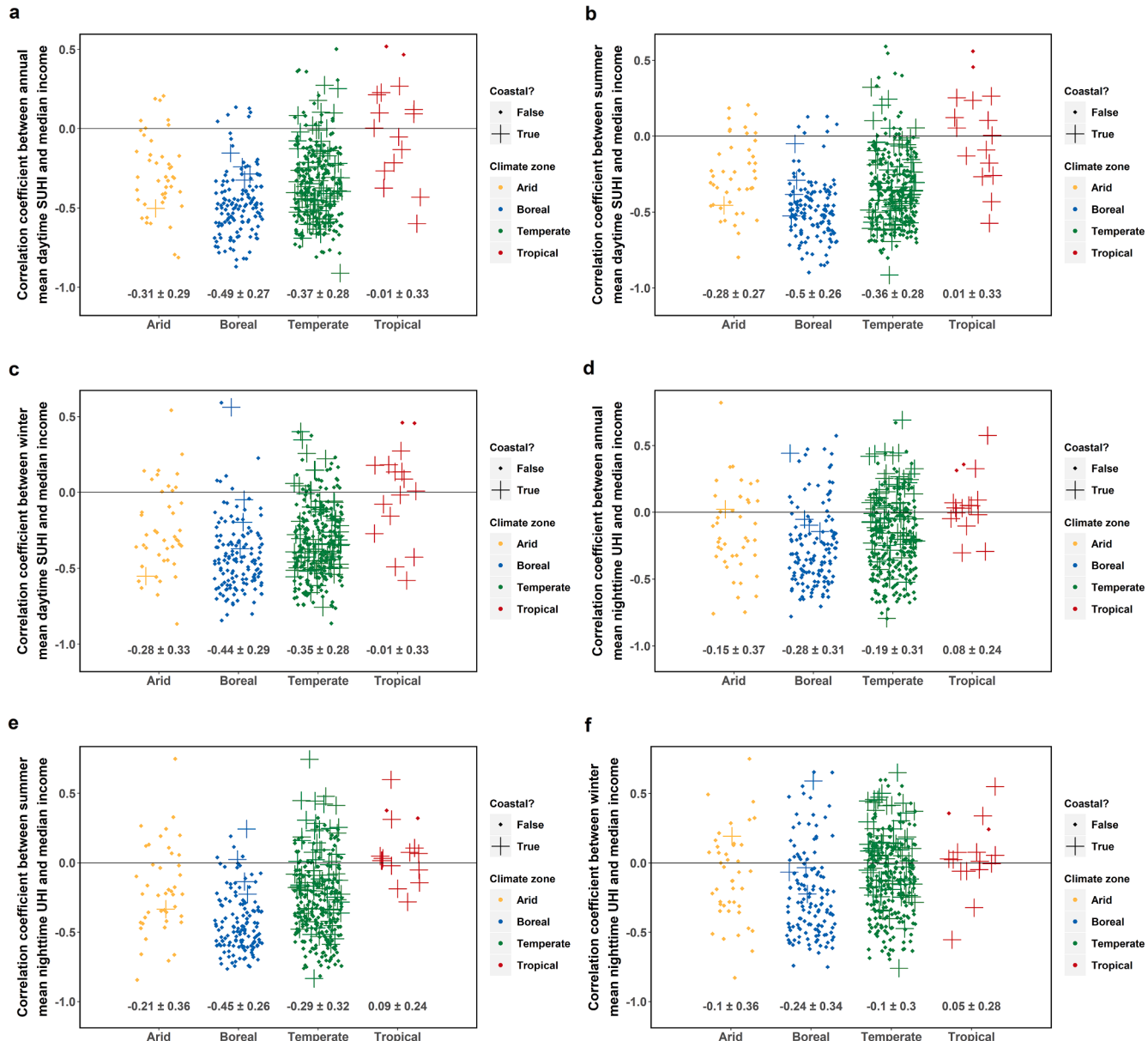


Fig. 5. Summary of intra-urban and inter-urban correlation of 2013–2017 (a) mean annual daytime SUHI, (b) mean summer daytime SUHI, (c) mean winter daytime SUHI, (d) mean annual nighttime SUHI, (e) mean summer nighttime SUHI, and (f) mean winter nighttime SUHI with 2017 median income. The points show the distribution (jittered) of the Pearson correlation coefficient (r) between the two variables for every US urbanized area divided into the climate zones, calculated from the census tract-level calculations. The numbers below the points give the mean and standard deviation of r after Fisher's z transformation and back-transformation.

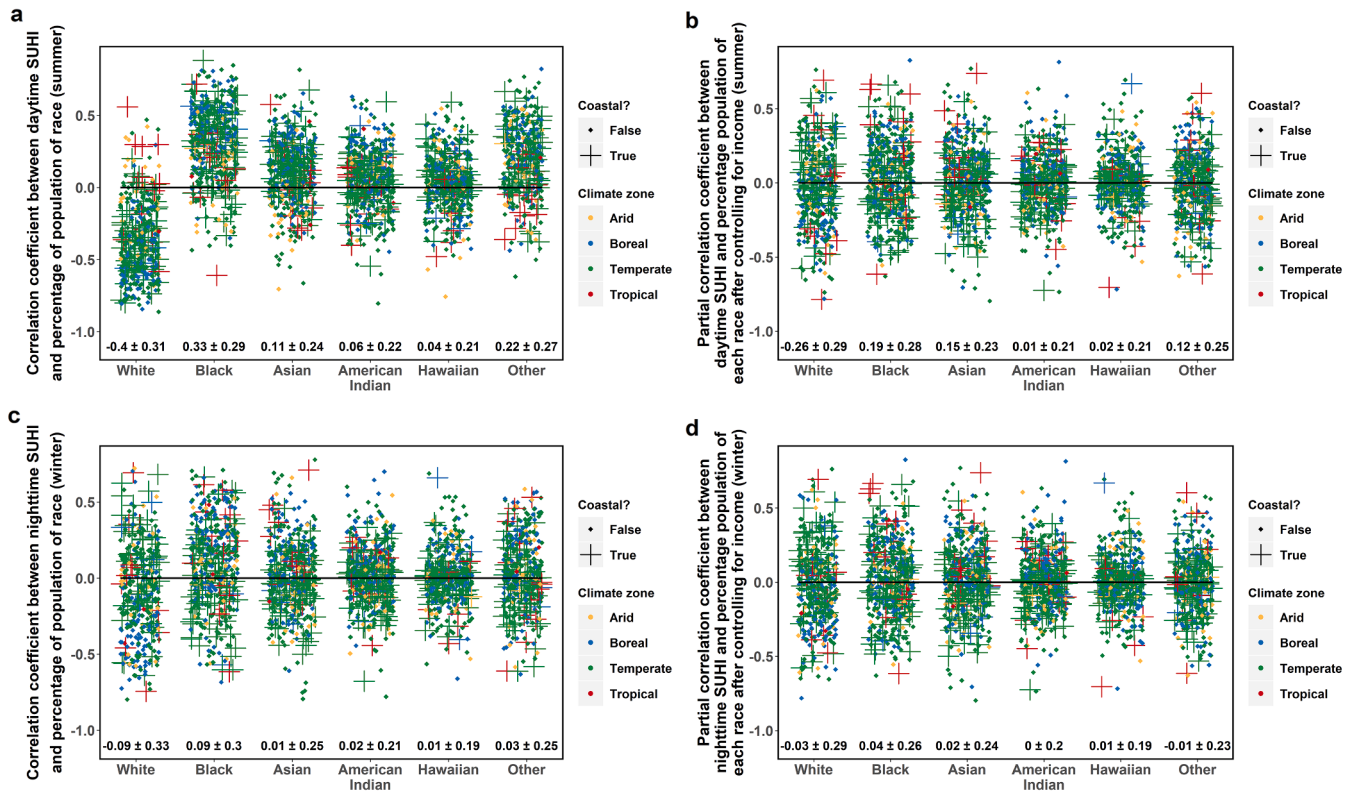


Fig. 6. Summary of intra-urban correlation of 2013–2017 mean (a) summer daytime and (c) winter nighttime SUHI with percentage of population belonging to each race. The points show the distribution (jittered) of the Pearson correlation coefficient (r) between the two variables for every US urbanized area divided into the climate zones, calculated from the census tract-level calculations. The numbers below the points give the mean and standard deviation of r after Fisher's z transformation and back-transformation. (b) and (d) Same as sub-figures (a) and (c), but for the partial correlation coefficients after accounting for median income.

- ii) NDVI is not a perfect proxy for all types of urban vegetation, particularly with reference to their local cooling potential; and
- iii) Discrepancies between satellite-derived LST, near-surface T_a , and heat stress.

Here we explain these in more detail, discussing the pros and cons of alternative methods and evaluating sensitivity of the results to the inherent assumptions in our approach.

The calculated SUHI and Δ NDVI values are only valid for clear-sky conditions and do not represent the climatological mean state. Moreover, the temporal and spatial patterns of cloud cover can introduce systematic biases in the clear-sky estimates if daily MODIS observations are used (Hu and Brunsell, 2013). We reduce this bias by using 8-day composites instead of the daily scenes when aggregating to annual and seasonal time scales. We illustrate the impact of this bias adjustment by calculating the percentage of valid data for both urban and rural pixels for each climate zone using 8-day LST composites and the daily LST product (Tables 3, S2–S4).

In general, the highest percentages of available data are over arid urbanized areas since they are relatively cloud free, with the lowest percentages over boreal and tropical climates. Although this distribution is consistent for both 8-day composites and daily scenes, the percentage of available LST data are much lower at the daily scale. Note that missing data are due to both cloudy pixels and the 3°C uncertainty limit specified during quality control. We generally expect similar percentages of valid pixels across the different climate zones for NDVI.

Even though the use of 8-day composites instead of daily scenes could also lead to biases in our SUHI estimates (Hu and Brunsell, 2013), we find surprisingly strong correlations between SUHI intensities calculated from the two levels of temporal aggregation, with r^2 over 0.90 and the slope of the linear fit close to 1 in most cases (Fig. 7). Exceptions include winter daytime and annual nighttime, with the largest

deviations seen for the boreal climate. Noting that the mean percentage of valid urban pixels for winter daytime for the boreal climate is only 17.9% (39.6% for annual nighttime) when using the daily scenes (66.6% when using 8-day composites; 94.3% for annual nighttime), we are more confident in the representativeness of the 8-day composites for calculating clear-sky SUHI estimates. Low missing data in the daily LST product in Table S3 (for instance, in the arid zone) is also a good proxy for regions and seasons for which our clear-sky estimates would approach the true LST climatology. This variability in representativeness across seasons and climate zones should be kept in mind when using this dataset.

The use of NDVI as a proxy for vegetation cover may be inaccurate, particularly during winter and for coastal regions, due to the influence of water bodies, snow cover, and clouds. These influences could introduce noise in urban–rural differentials, since the Δ NDVI signal can be small in some urbanized areas. Moreover, Δ NDVI may not always map linearly to local cooling due to vegetation. NDVI is an aggregate measure of live green vegetation. While all types of vegetation can increase evaporation, the cooling potential of different kinds of vegetation also vary, with trees also contributing to local cooling by providing shade (Leuzinger et al., 2010).

To illustrate the possible discrepancies between our quality-controlled clear-sky estimates of Δ NDVI and a more direct measure of the urban–rural vegetation differential, we examine its correlation with Δ Tree Cover from the NLCD dataset at the annual scale (Coulston et al., 2012; Fig. 8). While we do find relatively strong correlations between the two for all and non-coastal urbanized areas, there are regional anomalies. For tropical and arid zones, the associations are weak; and the overall correlations are low for coastal urbanized areas. In contrast, the correlations are high across the board for boreal climate. NDVI incorporates information about several kinds of live vegetation, not just trees. Accordingly, we should not expect strong correlations for regions

Table 3

Percentage of processed 8-day composite MODIS images (mean \pm standard deviation) for urban pixels for the cases and climate zones considered in the present study.

		Regions of interest			
Period	Case	Arid	Boreal	Temperate	Tropical
Annual daytime (%)	All	98.1 \pm 2.3	87.8 \pm 4.2	94.6 \pm 2.9	91.5 \pm 3.9
	Coastal	99.4 \pm 0	92.6 \pm 1.4	95.2 \pm 2.5	91.3 \pm 4.2
	Non-Coastal	98.1 \pm 2.3	87.7 \pm 4.2	94.4 \pm 3	92.9 \pm 1.1
	All	98.7 \pm 1.5	94.3 \pm 3.6	95.5 \pm 2.6	96.9 \pm 1.3
	Coastal	96.5 \pm 0	97 \pm 1	96 \pm 2	96.9 \pm 1.4
	Non-Coastal	98.7 \pm 1.5	94.2 \pm 3.7	95.4 \pm 2.7	97.3 \pm 0.5
Summer daytime (%)	All	99.8 \pm 1.1	98.1 \pm 2.1	94.5 \pm 5.9	89 \pm 7.2
	Coastal	99.5 \pm 0	97.3 \pm 2.4	94 \pm 6.2	88.5 \pm 7.5
	Non-Coastal	99.8 \pm 1.1	98.1 \pm 2	94.6 \pm 5.8	92.9 \pm 1.6
	All	99.2 \pm 1.5	97.8 \pm 1.9	96.5 \pm 3.2	96.9 \pm 2.3
	Coastal	91.3 \pm 0	96 \pm 4.6	96 \pm 2.8	96.7 \pm 2.5
	Non-Coastal	99.4 \pm 0.9	97.9 \pm 1.8	96.7 \pm 3.3	98.1 \pm 0.9
Winter daytime (%)	All	95 \pm 5.4	66.6 \pm 12.7	90.6 \pm 7.4	96.9 \pm 2.2
	Coastal	99.2 \pm 0	82.8 \pm 6.9	92.8 \pm 4.8	96.7 \pm 2.2
	Non-Coastal	94.9 \pm 5.4	66.1 \pm 12.5	90 \pm 7.9	98.7 \pm 0.7
	All	97.2 \pm 3.2	86.7 \pm 9.7	91.5 \pm 6.6	99.1 \pm 1.4
	Coastal	99.2 \pm 0	94.2 \pm 2.9	94.1 \pm 4.2	99 \pm 1.5
	Non-Coastal	97.2 \pm 3.3	86.4 \pm 9.7	90.8 \pm 6.9	99.9 \pm 0.1

with other types of urban vegetation.

Δ NDVI derived from the 8-day MODIS reflectance product also has a couple of advantages compared to the NLCD dataset. It provides information about the other forms of urban vegetation that may be relevant for the total evaporative cooling over urban green space and allows one to examine the seasonal components of the urban–rural vegetation differentials (the NLCD dataset is only for annual mean values).

Although LST and T_a are strongly correlated at longer time scales, they may not be correlated as strongly seasonally and/or spatially (Arnfield, 2003; Voogt and Oke, 2003; Chakraborty et al., 2017; Hu et al., 2019). Moreover, satellite-derived estimates of urban LST do not correspond to the T_a felt by urban pedestrians since they are influenced by roof top temperatures. Similarly, the temperature of the top of the tree is usually higher than the temperature under its shade (Leuzinger et al., 2010), suggesting that negative statistical correlations between LST and NDVI may underestimate the cooling effect of covered canopies. In the US, CUHI, which is directly related to T_a , is generally higher than the SUHI intensities derived from MODIS AQUA measurements for daytime, but show similar values during nighttime (Zhang et al., 2014). Consequently, satellite-derived LST has been associated with negative health outcomes at night (Laaidi et al., 2012), although it is not ideal for describing urban heat exposure under all conditions (Stone et al., 2019).

Even T_a is not adequate for this purpose, since heat stress is a function of many other variables (Oleson et al., 2018). Combinations of T_a , humidity, wind speed, and radiation have been used to create several different metrics and indices for heat stress, including apparent temperature, wet-bulb temperature, Universal Thermal Climate Index (UTCI), Human Thermal Comfort Index (HTCI), Physiological

Equivalent Temperature Index (PET), etc. (Harlan et al., 2006; Anderson et al., 2013; Pantavou et al., 2018). In the context of heat mitigation, the effect of urban vegetation may also be different for LST, T_a , and heat stress (Declet-Barreto et al., 2013; Chatterjee et al., 2019).

Insufficient measurement of T_a inside city boundaries, let alone other variables needed to predict heat stress at high resolutions, makes cross-city comparisons of disparities in urban heat stress difficult. Though studies on individual cities have suggested that intra-urban variations can lead to higher T_a and HTCI in neighborhoods inhabited by poorer and more vulnerable populations in the US (Harlan et al., 2006; Voelkel et al., 2018), further research is necessary to establish whether the disparities in them across US cities is as systematic as we see for SUHI.

Nevertheless, LST can still be an important input to predict T_a (and possibly heat stress), particularly with the recent growth in crowd-sourced meteorological data (Venter et al., 2020). Several efforts have been made to leverage satellite-derived LST to inform epidemiological studies (Kloog, 2019). Given the spatial continuity of satellite products and the logistical barriers to establishing dense measurement networks in cities, satellite-based LST can be a useful screening tool that complements more intensive human-health focused approaches. Looking beyond observations, numerical weather prediction models have the capacity to simulate T_a , LST, and more appropriate metrics of heat stress at relevant scales (Krayenhoff et al., 2018). These may be more useful for testing scenarios that cannot be explicitly measured, though they also have limitations pertaining to model simplifications and the accuracy of provided boundary conditions.

4.2. SUHI intensity, urban vegetation, and population distributions

The SUHI intensity is typically higher for the urban core, while income distribution within cities depends strongly on sociocultural context. For the US, this distribution is partly a result of a history of urban and national-scale policies, and stems from, among other things, urban flight, redlining, and access to public transportation (Kahn et al., 2008; Hoffman et al., 2020). Here we demonstrate an example case of disparity in SUHI intensity for a single nation, thus partly controlling for the variabilities in those sociocultural factors. For the US, these factors have generally led to higher poverty in city centers, with the population becoming richer and whiter as one moves towards the suburbs (Kahn et al., 2008). While this income and race-based segregation within cities has weakened over time (Juday, 2015), the higher SUHI for the urban core partly explains the associations between SUHI intensity, income, and race. Physical factors may also control the disparity in SUHI, particularly urban vegetation, which is also associated with income and race (Chakraborty et al., 2019; Nesbitt et al., 2019). We see positive correlations between Δ NDVI and median income (Fig. 7a, b, and 8c), implying richer urban residents live in ‘greener’ census tracts. However, for coastal urbanized areas, we see weaker correlations between Δ NDVI and median income ($r = 0.28 \pm 0.30$ for coastal and -0.45 ± 0.29 for non-coastal urbanized areas for the year; $r = 0.27 \pm 0.30$ for coastal and -0.46 ± 0.30 for non-coastal urbanized areas for summer), which is not surprising since ocean-adjacent census tracts, which tend to have less vegetation cover (Table 2), generally house richer populations.

We separated the difference in summer and winter NDVI for the low-income tracts (below 25 percentile of income) and high-income tracts (above 75 percentile of income) for each urbanized area (Fig. 9d). We find that this mean difference (of summer NDVI–winter NDVI) is greater in high income tracts for temperate and boreal climate zones ($p < 0.01$), but not for arid and tropical climate. This heterogeneity is due to the stronger vegetation phenology in temperate and boreal climate due to the larger abundance of deciduous trees and shrubs. Similar values in the difference in summer and winter NDVI in both low and high-income tracts for tropical and arid cases explain the practically non-varying relationships between daytime SUHI intensity and median income for urbanized areas in these climate zones. Similarly, the difference between summer and winter NDVI is significantly ($p < 0.01$) higher for white-

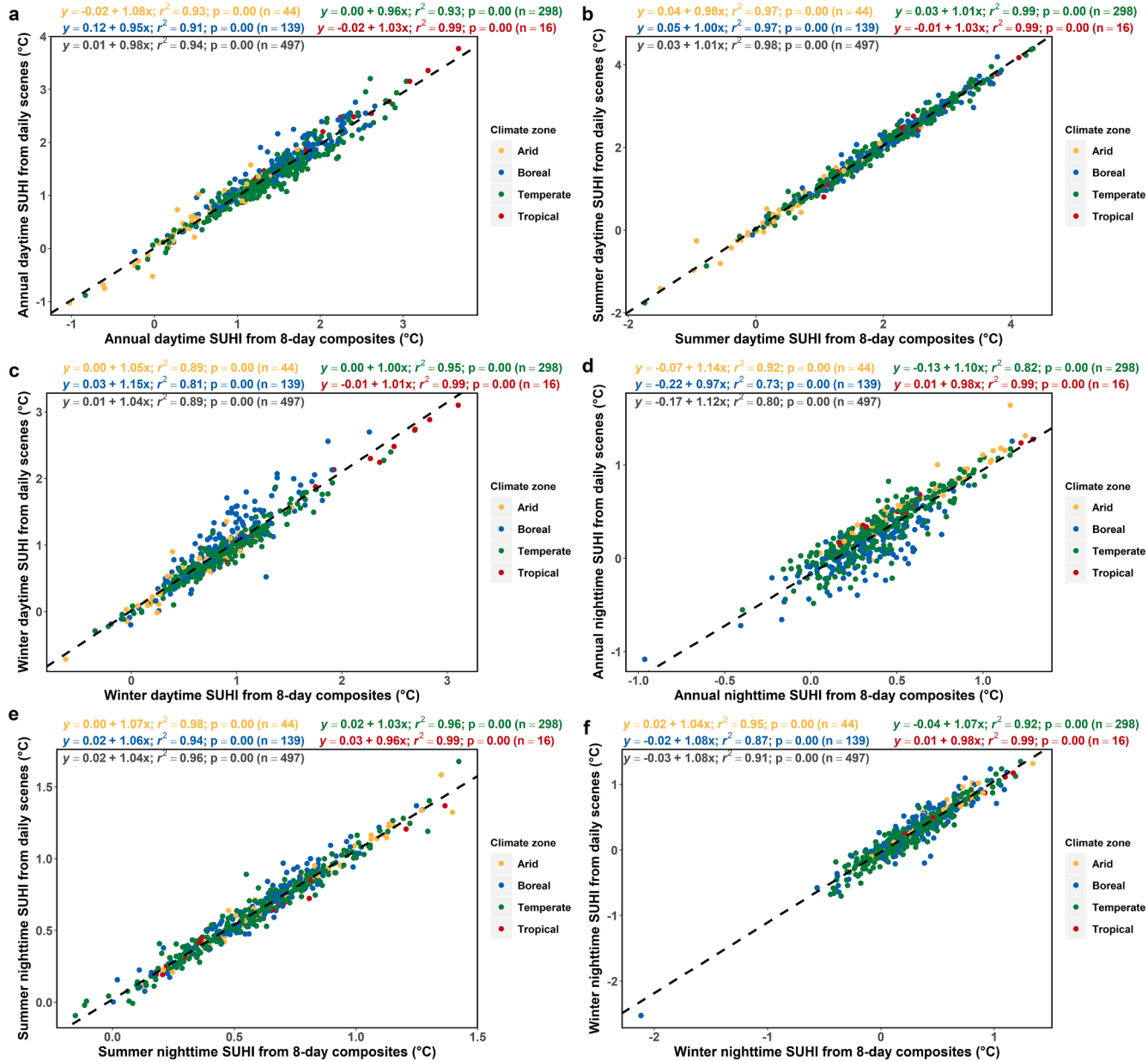


Fig. 7. Correlation between 2013 and 2017 estimates of (a) annual daytime, (b) summer daytime, (c) winter daytime, (d) annual nighttime, (e) winter nighttime, and (f) winter nighttime SUHI intensity from MODIS daily scenes and 8-day composites. The equations at the top show the correlations between the variables, calculated from the mean for each urbanized area (in black) and also sub-divided into the climate zones. The dashed line shows the best fit between the two variables for all urbanized areas.

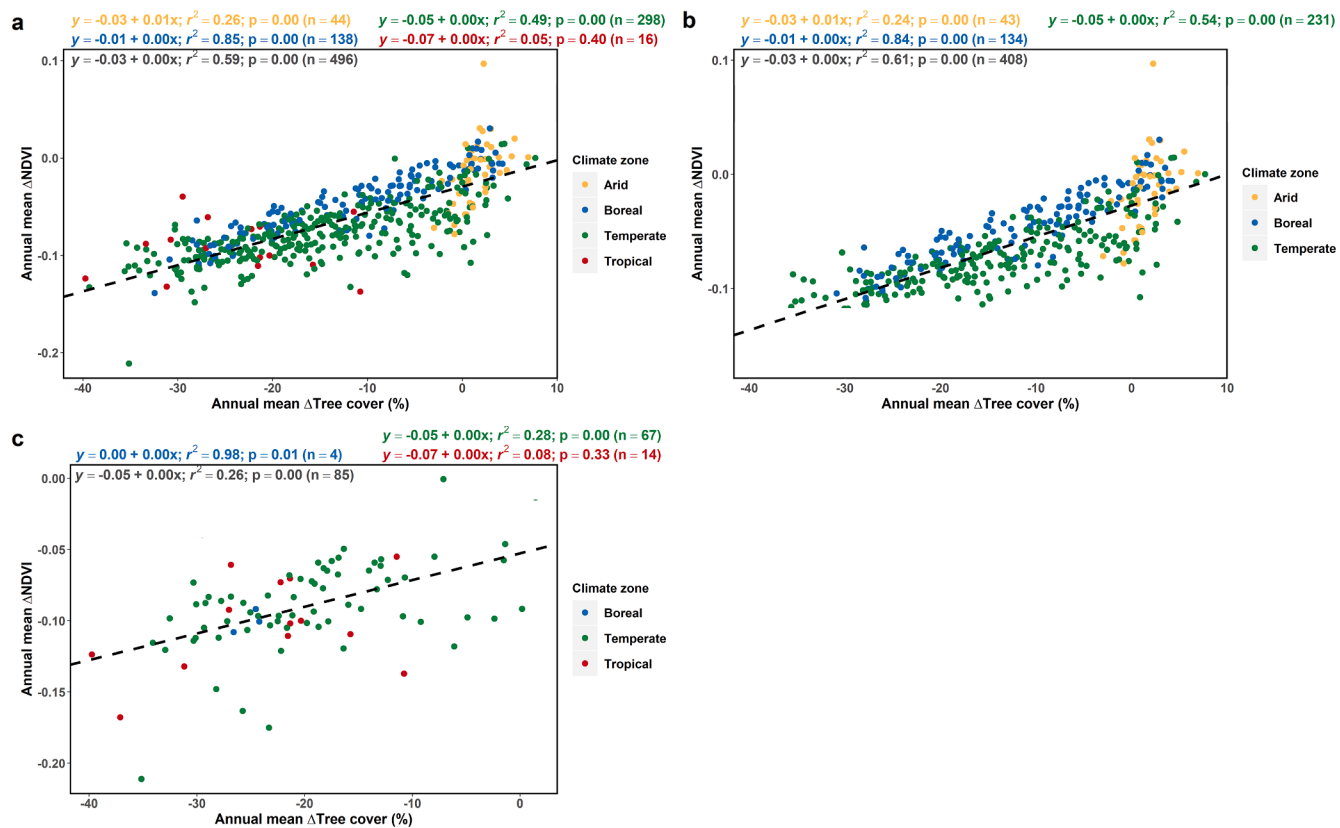


Fig. 8. Evaluation of urban–rural differential in NDVI (Δ NDVI) used in the present study for 2013–2017 and urban–rural differential in tree cover percentage from the NLCD dataset for 2013 for, (a) all urbanized areas, (b) non-coastal urbanized areas and, (c) coastal urbanized areas. The equations at the top show the correlations between the variables, calculated from the mean for each urbanized area (in black) and also sub-divided into the climate zones. The dashed line shows the best fit between the two variables for all urbanized areas.

dominant tracts (over 75% white residents) than non-white dominant tracts (under 25% white residents) for temperate and boreal climate.

4.3. Implications

The UHI is not an additional environmental stressor due to urbanization under all circumstances, since in some cases, especially in boreal climate and winter nights, a higher temperature may be preferable (Yang and Bou-Zeid, 2018). As we note from Fig. 5, the negative association between SUHI and median income is much weaker at night, practically disappearing during winter. For many US urban areas, since we can reasonably assume that the UHI has primarily negative health effects during summer days and primarily positive health effects during winter nights, our results imply that poor people may be suffering the adverse effects of the UHI without reaping the potential wintertime benefits. This result holds for race as well, with lower potential SUHI intensity for white-dominant census tracts during summer days and a relatively even distribution of SUHI intensity regardless of race for winter nights (Fig. 6). It is important to note however, that verifying the possible health connotations of these trends requires using more comprehensive metrics than LST. Although Laaidi et al. (2012) found nighttime LST to be associated with increased mortality during a heatwave period, it should be noted that T_a , which is more relevant to public health, is more strongly coupled with LST at nighttime, both within cities and on larger scales (Kawashima et al., 2000; Vancutsem et al., 2010; Zhang et al., 2011; Zhang et al., 2014). In this context, it is also important to stress that a lack of UHI does not imply no need for heat mitigation, the most striking example of this being cities situated in deserts with generally low (even negative) UHI intensities and high absolute temperatures (Martilli et al., 2020).

Moving beyond public health consequences, since UHI generally reduces heating demand during winter and increases cooling demand during summer compared to a rural baseline (Santamouris, 2014), poor and non-white urban residents in the US may be disproportionately bearing the economic burden of UHI during both seasons, an aspect that could be further explored in comparative analysis based on an initial screening using the tool presented in this paper. With reference to these economic consequences, the SUHI, which is heavily influenced by roof and road temperatures, is also more directly relevant.

Evident from Fig. 9, seasonal trends in SUHI disparity are particularly strong for boreal and temperate urbanized areas in the US. It remains to be seen whether these patterns would be consistent for T_a (and thus CUHI), and urban heat stress. For the overall spatial disparities however, since CUHI also tends to be higher for the urban core (Basara et al., 2011; Schatz and Kucharik, 2015; Smoliak et al., 2015; Hardin et al., 2018) and given the general distribution of population in US cities (Kahn et al., 2008; Juday 2015), we do expect higher T_a and CUHI in poorer, and non-white dominant census tracts, though these disparities are probably less prominent than for SUHI. Regardless of the strength of the intra-urban variabilities, it is important to address possible environmental disparities in heat exposure within urbanized areas and across seasons. The methodologically consistent SUHI dataset generated in this study is constrained by US census-defined urbanized areas, which, from an administrative perspective, provides an important input for future research and applications.

5. Conclusions

Most SUHI characterizations are done using physical delineations of urban areas and their rural references. While this is ideal since SUHIs are

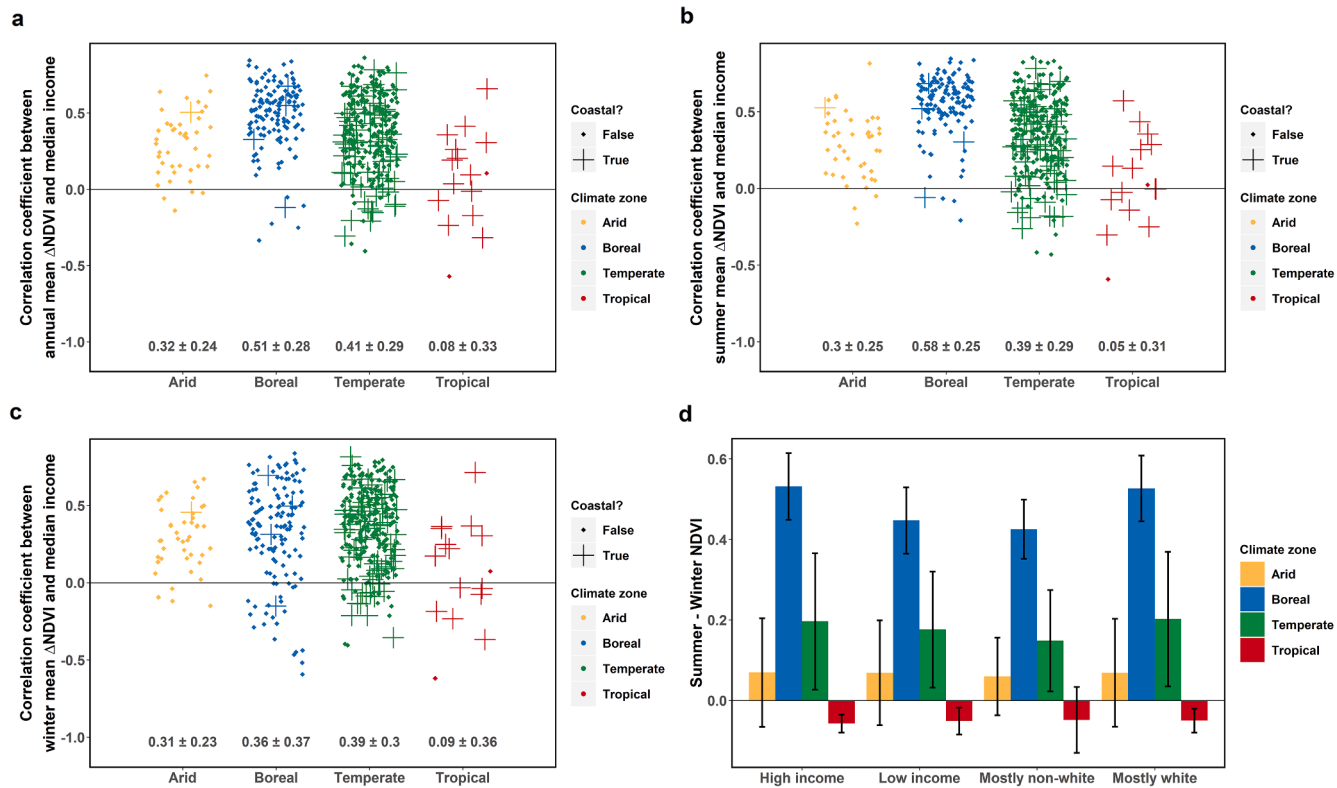


Fig. 9. Summary of intra-urban and inter-urban correlation of 2013–2017 (a) mean annual ΔNDVI , (b) mean summer ΔNDVI , and (c) mean winter ΔNDVI with 2017 median income. The points show the distribution (jittered) of the Pearson correlation coefficient (r) between the two variables for every US urbanized area divided into the climate zones, calculated from the census tract-level calculations. The numbers below the points give the mean and standard deviation of r after Fisher's z transformation and back-transformation. (d) Difference between summer and winter NDVI for high income (over 75 percentile for each urbanized area), low income (under 25 percentile for each urbanized area), mostly (over 75%) white, and mostly non-white (under 25% white) census tracts. The bars represent the composite means from all urbanized areas grouped into the four climate classes while the error bars represent the standard deviation for each case.

primarily due to changes in the physical characteristics of the land surface, the mismatch between physical boundaries and administrative boundaries makes comparisons between and within cities difficult. Here we use a fusion of remotely-sensed products and multiple administrative boundary definitions to characterize the intra and inter-city variation in the annual, summer, and winter SUHI intensities during daytime and nighttime in the US. We find that SUHI intensity is negatively correlated with income and percentage of white population for the vast majority of the urbanized areas. Moreover, poorer and non-white urban residents tend to be exposed to higher summer daytime SUHI, when heat stress would be at its maximum, and similar winter nighttime SUHI, when poorer urban residents could potentially benefit from higher ambient temperatures. Since SUHI intensity, its seasonality, and spatial variability are strongly associated with the degree of vegetation cover in and within urbanized areas, strategically placing urban parks and green spaces can be a useful way to reduce both the mean SUHI, as well as its spatial variability. The dataset created in this study can be accessed through the web application <https://datadrivenlab.users.earthengine.app/view/usuhiaapp>, and companion dataset Chakraborty et al. (2020).

Declaration of Competing Interest

The authors declare that they have no known competing financial interests or personal relationships that could have appeared to influence the work reported in this paper.

Acknowledgements

This work was funded by the Samuel Center for Social Connectedness (grant number: AWDR14157) and the National University of Singapore

Early Career Award (grant number: US_ECRA_FY18_P15). We thank Nicholas Chin of Yale-NUS College for assistance in extracting US census data, and Barkley Dai of Yale College for compiling an early version of the United States SUHI Explorer tool in Google Earth Engine.

Appendix A. Supplementary data

Supplementary data to this article can be found online at <https://doi.org/10.1016/j.isprsjprs.2020.07.021>.

References

- Anderson, G.B., Bell, M.L., Peng, R.D., 2013. Methods to calculate the heat index as an exposure metric in environmental health research. *Environ. Health Perspect.* 121 (10), 1111–1119.
- Arnfield, A.J., 2003. Two decades of urban climate research: a review of turbulence, exchanges of energy and water, and the urban heat island. *Int. J. Climatol.: J. Roy. Meteorol. Soc.* 23 (1), 1–26.
- Basara, J.B., Illston, B.G., Fiebrich, C.A., Browder, P.D., Morgan, C.R., McCombs, A., Crawford, K.C., 2011. The Oklahoma city micronet. *Meteorol. Appl.* 18 (3), 252–261.
- Bontemps, S., Defourny, P., Radoux, J., Van Bogaert, E., Lamarche, C., Achard, F., Züllkhe, M., 2013 Consistent global land cover maps for climate modelling communities: current achievements of the ESA's land cover CCI. In: Proc. ESA Living Planet Symp. pp. 9–13.
- Chakraborty, T., Sarangi, C., Tripathi, S.N., 2017. Understanding diurnality and inter-seasonality of a sub-tropical urban heat island. *Bound.-Layer Meteorol.* 163 (2), 287–309.
- Chakraborty, T., Lee, X., 2019. A simplified urban-extent algorithm to characterize surface urban heat islands on a global scale and examine vegetation control on their spatiotemporal variability. *Int. J. Appl. Earth Obs. Geoinf.* 74, 269–280.
- Chakraborty, T., Hsu, A., Manya, D., Sheriff, G., 2019. Disproportionately higher exposure to urban heat in lower-income neighborhoods: a multi-city perspective. *Environ. Res. Lett.* 14 (10), 105003.
- Chakraborty, T., Hsu, A., Sheriff, G., Manya, D., 2020. United States Surface Urban Heat Island database. Mendeley Data, V2, 10.17632/x9mv4krnm2.2.

- Chatterjee, S., Khan, A., Dinda, A., Mithun, S., Khatun, R., Akbari, H., Wang, Y., 2019. Simulating micro-scale thermal interactions in different building environments for mitigating urban heat islands. *Sci. Total Environ.* 663, 610–631.
- Clark, L.P., Millet, D.B., Marshall, J.D., 2014. National patterns in environmental injustice and inequality: outdoor NO₂ air pollution in the United States. *PLoS ONE* 9 (4), e94431.
- Clinton, N., Gong, P., 2013. MODIS detected surface urban heat islands and sinks: global locations and controls. *Remote Sens. Environ.* 134, 294–304.
- Coulston, John W., Moisen, Gretchen G., Wilson, Barry T., Finco, Mark V., Cohen, Warren B., Brewer, C. Kenneth, 2012. Modeling percent tree canopy cover: a pilot study. *Photogramm. Eng. Remote Sens.* 78 (7), 715–727. <https://doi.org/10.14358/PERS.78.7.715>.
- Cui, Y.Y., De Foy, B., 2012. Seasonal variations of the urban heat island at the surface and the near-surface and reductions due to urban vegetation in Mexico City. *J. Appl. Meteorol. Climatol.* 51 (5), 855–868.
- Dadvand, P., Nieuwenhuijsen, M.J., Esnaola, M., Forns, J., Basagaña, X., Alvarez-Pedrerol, M., Jerrett, M., 2015. Green spaces and cognitive development in primary schoolchildren. *Proc. Natl. Acad. Sci.* 112 (26), 7937–7942.
- Danielson, J.J., Gesch, D.B., 2011. Global multi-resolution terrain elevation data 2010 (GMTED2010). US Department of the Interior, US Geological Survey, p. 26.
- Decler-Barreto, J., Brazel, A.J., Martin, C.A., Chow, W.T., Harlan, S.L., 2013. Creating the park cool island in an inner-city neighborhood: heat mitigation strategy for Phoenix, AZ. *Urban Ecosyst.* 16 (3), 617–635.
- De Dios, V.R., Roy, J., Ferrio, J.P., Alday, J.G., Landais, D., Milcu, A., Gessler, A., 2015. Processes driving nocturnal transpiration and implications for estimating land evapotranspiration. *Sci. Rep.* 5, 10975.
- Fong, K.C., Hart, J.E., James, P., 2018. A review of epidemiologic studies on greenness and health: updated literature through 2017. *Curr. Environ. Health Rep.* 5 (1), 77–87.
- Gorelick, N., Hancher, M., Dixon, M., Ilyushchenko, S., Thau, D., Moore, R., 2017. Google Earth Engine: planetary-scale geospatial analysis for everyone. *Remote Sens. Environ.* 202, 18–27.
- Hardin, A.W., Liu, Y., Cao, G., Vanos, J.K., 2018. Urban heat island intensity and spatial variability by synoptic weather type in the northeast US. *Urban Clim.* 24, 747–762.
- Harlan, S.L., Brazel, A.J., Prashad, L., Stefanov, W.L., Larsen, L., 2006. Neighborhood microclimates and vulnerability to heat stress. *Soc. Sci. Med.* 63 (11), 2847–2863.
- Heaviside, C., Macintyre, H., Vardoulakis, S., 2017. The Urban Heat Island: implications for health in a changing environment. *Curr. Environ. Health Rep.* 4 (3), 296–305.
- Hoffman, J.S., Shandas, V., Pendleton, N., 2020. The effects of historical housing policies on resident exposure to intra-urban heat: a study of 108 US urban areas. *Climate* 8 (1), 12.
- Hsu, A., Alexandre, N., Brandt, J., Chakraborty, T., Comess, S., Feierman, A., ... Moyo, N., 2018. The Urban Environment and Social Inclusion Index. Yale University, New Haven, CT. Available: datadrivenlab.org/urban.
- Hsu, A., Sheriff, G., Chakraborty, T., Manya, D., under review. Urban heat island inequalities by race and income in major US cities.
- Hu, L., Brunsell, N.A., 2013. The impact of temporal aggregation of land surface temperature data for surface urban heat island (SUHI) monitoring. *Remote Sens. Environ.* 134, 162–174.
- Hu, L., Monaghan, A., Voogt, J.A., Barlage, M., 2016. A first satellite-based observational assessment of urban thermal anisotropy. *Remote Sens. Environ.* 181, 111–121.
- Hu, Y., Hou, M., Jia, G., Zhao, C., Chen, X., Xu, Y., 2019. Comparison of surface and canopy urban heat islands within megacities of eastern China. *ISPRS J. Photogramm. Remote Sens.* 156, 160–168.
- Imhoff, M.L., Zhang, P., Wolfe, R.E., Bounoua, L., 2010. Remote sensing of the urban heat island effect across biomes in the continental USA. *Remote Sens. Environ.* 114 (3), 504–513.
- Iyer, H.S., Valeri, L., James, P., Chen, J.T., Hart, J.E., Laden, F., Rebbeck, T.R., 2020. The contribution of residential greenness to mortality among men with prostate cancer: a registry-based cohort study of Black and White men. *Environ. Epidemiol.* 4 (2), e087.
- Juday, L.J., 2015. The changing shape of American cities. Charlottesville: Demographics Research Group, Weldon Cooper Center for Public Service; University of Virginia.
- Kahn, M. E., Glaeser, E., Rappaport, J., 2008. Why do the poor live in cities? The role of public transportation. Schola. Regional relationships between surface temperature, vegetation, and human settlement in a rapidly urbanizing ecosystem rly Articles 2958224, Harvard University Department of Economics.
- Kawashima, S., Ishida, T., Minomura, M., Miwa, T., 2000. Relations between surface temperature and air temperature on a local scale during winter nights. *J. Appl. Meteorol.* 39 (9), 1570–1579.
- Kloog, I., 2019. Use of earth observations for temperature exposure assessment in epidemiological studies. *Curr. Opin. Pediatr.* 31 (2), 244–250.
- Krayenhoff, E.S., Moustaqai, M., Broadbent, A.M., Gupta, V., Georgescu, M., 2018. Diurnal interaction between urban expansion, climate change and adaptation in US cities. *Nat. Clim. Change* 8 (12), 1097–1103.
- Lagourde, J.P., Moreau, P., Irvine, M., Bonnefond, J.M., Voogt, J.A., Sollier, F., 2004. Airborne experimental measurements of the angular variations in surface temperature over urban areas: case study of Marseille (France). *Remote Sens. Environ.* 93 (4), 443–462.
- Laaidi, K., Zeghnoun, A., Dousset, B., Bretin, P., Vandendorren, S., Giraudet, E., Beaudeau, P., 2012. The impact of heat islands on mortality in Paris during the August 2003 heat wave. *Environ. Health Perspect.* 120 (2), 254–259.
- Lai, J., Zhan, W., Huang, F., Quan, J., Hu, L., Gao, L., Ju, W., 2018. Does quality control matter? Surface urban heat island intensity variations estimated by satellite-derived land surface temperature products. *ISPRS J. Photogramm. Remote Sens.* 139, 212–227.
- Leuzinger, Sebastian, Vogt, Roland, Körner, Christian, 2010. Tree surface temperature in an urban environment. *Agric. For. Meteorol.* 150 (1), 56–62.
- Li, X., Zhou, Y., Asrar, G.R., Imhoff, M., Li, X., 2017. The surface urban heat island response to urban expansion: a panel analysis for the conterminous United States. *Sci. Total Environ.* 605, 426–435.
- Maimaitiyiming, M., Ghulam, A., Tiyip, T., Pla, F., Latorre-Carmona, P., Halik, Ü., Caetano, M., 2014. Effects of green space spatial pattern on land surface temperature: Implications for sustainable urban planning and climate change adaptation. *ISPRS J. Photogramm. Remote Sens.* 89, 59–66.
- Manoli, G., Faticchi, S., Schläpfer, M., Yu, K., Crowther, T.W., Meili, N., Bou-Zeid, E., 2019. Magnitude of urban heat islands largely explained by climate and population. *Nature* 573 (7772), 55–60.
- Manoli, G., Faticchi, S., Bou-Zeid, E., Katul, G.G., 2020a. Seasonal hysteresis of surface urban heat islands. *Proc. Natl. Acad. Sci.*
- Manoli, G., Faticchi, S., Schläpfer, M., Yu, K., Crowther, T. W., Meili, N., ... Zeid, E.B., 2020b. Reply to Martilli et al. (2020): Summer average urban-rural surface temperature differences do not indicate the need for urban heat reduction. [10.31219/osf.io/mwpna](https://doi.org/10.31219/osf.io/mwpna).
- Martilli, A., Krayenhoff, E.S., Nazarian, N., 2020a. Is the urban heat island intensity relevant for heat mitigation studies? *Urban Clim.* 31, 100541.
- Martilli, A., Roth, M., Chow, W.T., Demuzere, M., Lipson, M., Krayenhoff, E.S., ... Hart, M.A., 2020b. Summer average urban-rural surface temperature differences do not indicate the need for urban heat reduction. [10.31219/osf.io/8gnbf](https://doi.org/10.31219/osf.io/8gnbf).
- Mather, M., Rivers, K.L., Jacobsen, L.A., 2005. The American community survey. *Popul. Bull.* 60 (3), 1–20.
- Muller, C.L., Chapman, L., Grimmond, C.S.B., Young, D.T., Cai, X., 2013. Sensors and the city: a review of urban meteorological networks. *Int. J. Climatol.* 33 (7), 1585–1600.
- Nesbitt, L., Meitner, M.J., Girling, C., Sheppard, S.R., Lu, Y., 2019. Who has access to urban vegetation? A spatial analysis of distributional green equity in 10 US cities. *Landscape Urban Plann.* 181, 51–79.
- Niu, L., Tang, R., Jiang, Y., Zhou, X., 2020. Spatiotemporal patterns and drivers of the surface urban heat island in 36 major cities in China: a comparison of two different methods for delineating rural areas. *Sustainability* 12 (2), 478.
- Nowak, D.J., Dwyer, J.F., 2007. Understanding the benefits and costs of urban forest ecosystems. In: *Urban and Community Forestry in the Northeast*. Springer, Dordrecht, pp. 25–46.
- Oleson, K.W., Anderson, G.B., Jones, B., McGinnis, S.A., Sanderson, B., 2018. Avoided climate impacts of urban and rural heat and cold waves over the US using large climate model ensembles for RCP8. 5 and RCP4. 5. *Clim. Change* 146 (3–4), 377–392.
- Pantavou, K., Lykoudis, S., Nikolopoulou, M., Tsilos, I.X., 2018. Thermal sensation and climate: a comparison of UTCI and PET thresholds in different climates. *Int. J. Biometeorol.* 62 (9), 1695–1708.
- Peng, S., Piao, S., Ciais, P., Friedlingstein, P., Ottle, C., Bréon, F.M., Myneni, R.B., 2012. Surface urban heat island across 419 global big cities. *Environ. Sci. Technol.* 46 (2), 696–703.
- Rouse, J. Jr, Haas, R.H., Schell, J.A., Deering, D.W., 1974 Monitoring vegetation systems in the Great Plains with ERTS. NASA Goddard Space Flight Center 3DERTS-1 Symp. vol 1, pp. 309–317 section A.
- Rubel, F., Kottek, M., 2010. Observed and projected climate shifts 1901–2100 depicted by world maps of the Köppen-Geiger climate classification. *Meteorol Z.* 19, 135–141.
- Santamouris, M., 2014. On the energy impact of urban heat island and global warming on buildings. *Energy Build.* 82, 100–113.
- Santamouris, M., Haddad, S., Fiorito, F., Osmond, P., Ding, L., Prasad, D., Wang, R., 2017. Urban heat island and overheating characteristics in Sydney, Australia. An analysis of multiyear measurements. *Sustainability* 9 (5), 712.
- Schatz, J., Kucharik, C.J., 2015. Urban climate effects on extreme temperatures in Madison, Wisconsin, USA. *Environ. Res. Lett.* 10 (9), 094024.
- Smoliak, B.V., Snyder, P.K., Twine, T.E., Mykleby, P.M., Hertel, W.F., 2015. Dense network observations of the Twin Cities canopy-layer urban heat island. *J. Appl. Meteorol. Climatol.* 54 (9), 1899–1917.
- Stewart, I.D., 2011. A systematic review and scientific critique of methodology in modern urban heat island literature. *Int. J. Climatol.* 31 (2), 200–217.
- Stone Jr, B., Lanza, K., Mallen, E., Vargo, J., Russell, A., 2019. Urban heat management in Louisville, Kentucky: a framework for climate adaptation planning. *J. Plan. Educ. Res.* 0739456X19879214.
- Tan, J., Zheng, Y., Tang, X., Guo, C., Li, L., Song, G., Chen, H., 2010. The urban heat island and its impact on heat waves and human health in Shanghai. *Int. J. Biometeorol.* 54 (1), 75–84.
- Tessum, C.W., Apte, J.S., Goodkind, A.L., Muller, N.Z., Mullins, K.A., Paoletta, D.A., Hill, J.D., 2019. Inequity in consumption of goods and services adds to racial-ethnic disparities in air pollution exposure. *Proc. Natl. Acad. Sci.* 116 (13), 6001–6006.
- Vancutsem, C., Ceccato, P., Dinku, T., Connor, S.J., 2010. Evaluation of MODIS land surface temperature data to estimate air temperature in different ecosystems over Africa. *Remote Sens. Environ.* 114 (2), 449–465.
- Venter, Z.S., Brousse, O., Esau, I., Meier, F., 2020. Hyperlocal mapping of urban air temperature using remote sensing and crowdsourced weather data. *Remote Sens. Environ.* 242, 111791.
- Vermote, E.F., Kotchenova, S.Y., Ray, J.P., 2011. MODIS surface reflectance user's guide. MODIS Land Surface Reflectance Science Computing Facility, version, 1.
- Voelkel, J., Hellman, D., Sakuma, R., Shandas, V., 2018. Assessing vulnerability to urban heat: A study of disproportionate heat exposure and access to refuge by socio-demographic status in Portland, Oregon. *Int. J. Environ. Res. Public Health* 15 (4), 640.
- Voogt, J.A., Oke, T.R., 2003. Thermal remote sensing of urban climates. *Remote Sens. Environ.* 86 (3), 370–384.

- Wan, Zhengming, 2014. New refinements and validation of the collection-6 MODIS land-surface temperature/emissivity product. *Remote Sens. Environ.* 140, 36–45.
- Yang, J., Bou-Zeid, E., 2018. Should cities embrace their heat islands as shields from extreme cold? *J. Appl. Meteorol. Climatol.* 57 (6), 1309–1320.
- Yang, Q., Huang, X., Tang, Q., 2019. The footprint of urban heat island effect in 302 Chinese cities: temporal trends and associated factors. *Sci. Total Environ.* 655, 652–662.
- Zhang, K., Oswald, E.M., Brown, D.G., Brines, S.J., Gronlund, C.J., White-Newsome, J.L., O'Neill, M.S., 2011. Geostatistical exploration of spatial variation of summertime temperatures in the Detroit metropolitan region. *Environ. Res.* 111 (8), 1046–1053.
- Zhang, P., Bounoua, L., Imhoff, M.L., Wolfe, R.E., Thome, K., 2014. Comparison of MODIS land surface temperature and air temperature over the continental USA meteorological stations. *Canadian J. Remote Sens.* 40 (2), 110–122.
- Zhang, Q., Zhang, M., Zhou, W., Xu, W., Zhang, J., 2019. The influence of different urban and rural selection methods on the spatial variation of urban heat island intensity. In: IGARSS 2019-2019 IEEE International Geoscience and Remote Sensing Symposium. IEEE, pp. 4403–4406.
- Zhao, L., Lee, X., Smith, R.B., Oleson, K., 2014. Strong contributions of local background climate to urban heat islands. *Nature* 511 (7508), 216–219.
- Zhou, B., Rybski, D., Kropp, J.P., 2017. The role of city size and urban form in the surface urban heat island. *Sci. Rep.* 7 (1), 1–9.
- Zhou, D., Zhao, S., Zhang, L., Sun, G., Liu, Y., 2015. The footprint of urban heat island effect in China. *Sci. Rep.* 5, 11160.
- Ziter, C.D., Pedersen, E.J., Kucharik, C.J., Turner, M.G., 2019. Scale-dependent interactions between tree canopy cover and impervious surfaces reduce daytime urban heat during summer. *Proc. Natl. Acad. Sci.* 116 (15), 7575–7580.